Drug loaded cellulose–chitosan aerogel microfibers for wound dressing applications

Cellulose
https://doi.org/10.1007/s10570-022-04630-6

ORIGINAL RESEARCH

Drug loaded cellulose–chitosan aerogel microfibers for wound dressing applications

M. Rostamitabar · A. Ghahramani · G. Seide · S. Jockenhoevel · S. Ghazanfari

Received: 23 January 2022 / Accepted: 27 April 2022

Abstract Cellulose and chitosan have been studied for wound dressing due to their biocompatibility, biodegradability, lower antigenicity, and renewability. The functional and structural characteristics of such biopolymers can be dramatically improved by their transformation into fibrous bioaerogels due to their outstanding characteristics such as low density, high porosity, and large specific surface area. Producing aerogels in the form of fibers and textiles not only can enhance mechanical properties, stiffness, and shapeability of aerogels but also lead to short drying times and scalable production processes. Hereby, wet spun chitosan-cellulose aerogel microfibers (CHCLAFs) in two ratios of 1:5 and 1:10 have been produced by supercritical CO_2 ($scCO_2$) drying for wound dressing application. The fibers were also loaded with ibuprofen (IBU) through post-treatment $scCO_2$ impregnation. CHCLAF characteristics in terms of morphology, textural properties, thermal stability, mechanical properties, and in vitro assessment such as drug release, antibacterial properties, cytotoxicity, and wound exudate uptake were analyzed and compared to pure cellulose aerogel microfibers (CLF). Blended CHCLAFs showed a low density (~0.18 g/cm^3), high porosity (~85%), and large specific surface area (~300 m^2/g) with a macro-porous outer shell and a nano-porous inner core. The fibers were transformed into braided meshes that were highly water absorbable (~400 wt.%) and bactericidal against *escherichia coli* and *staphylococcus aureus*. Furthermore, the fibrous structures showed no cytotoxicity using fibroblast cells, and the hybrid fibers were able to release IBU over 48 h in a sustained manner. The results showed that the CHCLAFs could be used as a promising candidate for wound dressing materials.

M. Rostamitabar · G. Seide · S. Jockenhoevel · S. Ghazanfari (✉)
Faculty of Science and Engineering, Aachen-Maastricht Institute for Biobased Materials (AMIBM), Maastricht University, Urmonderbaan 22, 6167 RD Geleen, The Netherlands
e-mail: samaneh.ghazanfari@maastrichtuniversity.nl

M. Rostamitabar · A. Ghahramani · S. Jockenhoevel · S. Ghazanfari
Department of Biohybrid and Medical Textiles (BioTex), AME-Helmholtz Institute for Biomedical Engineering, RWTH Aachen University, Forckenbeckstrabe 55, 52072 Aachen, Germany

Published online: 11 June 2022

Graphical abstract

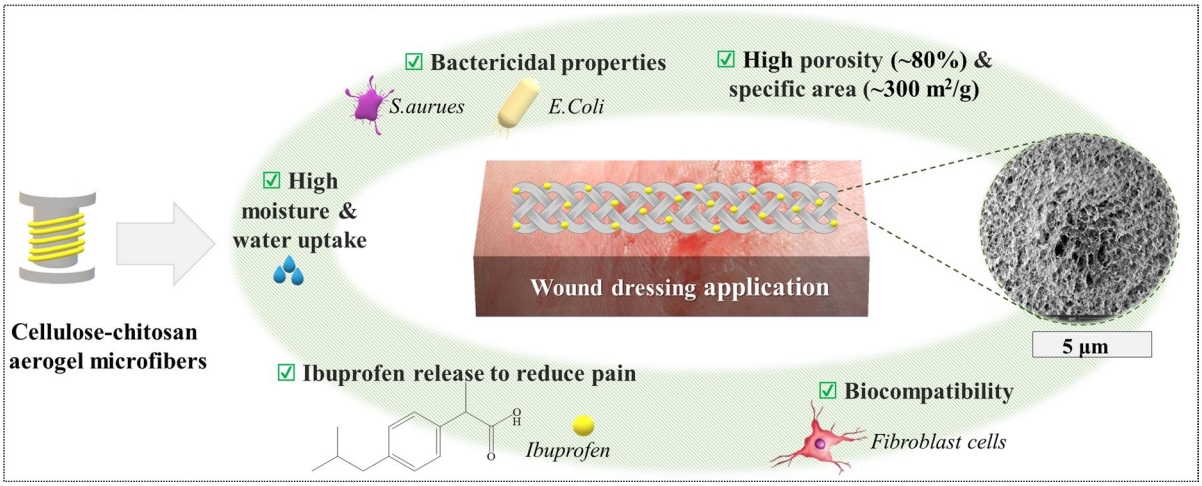

Keywords Cellulose · Chitosan · Microfiber · Aerogel · Wound dressing · Supercritical CO_2

Introduction

It has been forecast that the global wound dressing market can exceed $15 billion by 2022. Moreover, the advanced wound care market aiming for surgical wounds and chronic ulcers is expected to exceed $22 billion by 2024 (Sen 2019). Medical textile plays an important role in wound dressings, and such a continuing rise in the need for wounds products requires the fabrication of sustainable added-value products originating from renewable materials such as cellulose and chitosan (McQueen 2011; Rostamitabar et al. 2021a). Cellulose, the most abundant biopolymer present in plant cell walls, is made of β-D-glucose held by β-1, 4-glycosidic linkages (French 2017). Cellulose has been widely used in wound dressing products due to its high flexibility, excellent physical barrier for microbial pathogens, and especially its moisture-retaining properties thanks to the presence of numerous hydroxyl functional groups (Dassanayake et al. 2018; Yuan et al. 2021). Wounds are well known to heal more quickly in a moist environment since a sufficient supply of growth factors and other molecules to the healing tissues is more likely to happen (Sahana and Rekha 2018). Furthermore, cellulose can assist in the absorption of wound exudates evolving in the uptake of cell debris (Sulaeva et al. 2015; Sahana and Rekha 2018). However, cellulose by itself does not possess any antibacterial and antifungal properties, which can be a drawback for infectious wound sites.

Chitosan is the active form and deacetylated substance of chitin biomacromolecules made up of n-acetyl glucosamine residues held by β-1, 4 linkages. Chitin is a natural biopolymer that can be found in fungi, crustaceans, mollusks, and insects and has been widely investigated as an antimicrobial agent to prevent bacterial and fungal infections of the wound site (Bano et al. 2017; Fan et al. 2020). Chitosan has also exhibited fibroblast proliferative characteristics necessary to accelerate wound healing (Minagawa et al. 2007) and can lead to activation of polymorphonuclear leukocytes and macrophages for phagocytosis and expression of interleukin-1 (IL-1), transforming growth factor beta (TGF-β), and platelet-derived growth factor (PDGF) (Lin et al. 2013; Bano et al. 2017).

The functional and structural characteristics of such biopolymers can be dramatically enhanced by producing fibrous aerogels due to their outstanding characteristics such as low density, high porosity, and large specific surface area. Aerogels are produced from wet gels in delicate drying processes such as freeze-drying or supercritical CO_2 ($scCO_2$) so that the gel structure is merely conserved. In contrast to other drying techniques, $scCO_2$ is a mild temperature process that leads to better textural properties as well

as sterilization (Ribeiro et al. 2020) and drug loading possibilities of fabricated aerogels (Rostamitabar et al. 2021a). Drug impregnation in the aerogel fibers can be performed either during gel preparation or during the network formation (solvent exchange) or after drying the aerogel through the post-treatment method which utilizes $scCO_2$ as a medium to dissolve and impregnate the drug (Ulker and Erkey 2014). In addition, producing microfiber aerogels not only can enhance the mechanical properties, stiffness, and shapeability of aerogels but also lead to short $scCO_2$ drying times and scalable production processes (Rostamitabar et al. 2021b).

The design and fabrication of new biomaterials from renewable resources to promote the wound healing process are a constant demand from the health sector. To the best of our knowledge, no cellulose–chitosan hybrid aerogel in the geometry of microfiber or textile has been fabricated or studied for wound dressing application. Such bioaerogel microfibers have the combination of unique characteristics of biopolymers, microfibers, and aerogels in one single product. Moreover, these products have a great potential to be further functionalized and tuned for not only different types of wounds but also other biomedical applications.

In this study, cellulose–chitosan aerogel microfibers (CHCLAFs) were produced by blending microcrystalline cellulose (MCC) with low molecular weight chitosan powder (CHP) using $ZnCl_2{\cdot}3H_2O$ as a dissolving agent. This low-cost hydrated salt is able to simultaneously dissolve cellulose and chitosan and has the potential to be extended to industrial processes (Lin et al. 2012). Hybrid aerogel fibers in two different ratios of 1:10 and 1:5 (CHP:MCC), referred to as CH1CL10 and CH1CL5 respectively, were fabricated. Moreover, cellulose aerogel fibers (CLF) were created through a similar processing route to be compared with hybrid aerogel fibers. Ibuprofen (IBU) is an anti-inflammatory, non-steroidal analgesic, and antipyretic drug which can promote wound healing by preventing excessive inflammation. Fibers were loaded with IBU through $scCO_2$ post-treatment impregnation since the solubility of ibuprofen in $scCO_2$ is satisfactory as reported to be 0.98% (w/w) at 40 ± 1 °C and 180 ± 2 bar (Mehling et al. 2009).

CLF and CHCLAF characteristics were investigated in terms of morphology, physio-chemical structure, textural properties, thermal stability, mechanical properties, and in vitro assessments including humidity and water uptake, wound exudate uptake, drug release, cytotoxicity, and antibacterial properties.

Materials and methods

Materials

Microcrystalline cellulose (MCC) with the product number C6288 (degree of polymerization of 159) (Rostamitabar et al. 2021b), CHP (50–190 kDa, 75–85% deacetylated), dialysis tubing cellulose membrane (typical molecular weight cut-off = 14,000), dimethyl sulfoxide (DMSO), and cell proliferation kit II (XTT) were purchased from Sigma–Aldrich (Germany). $ZnCl_2$ (97%) and 4-Isobutyl-alpha-methylphenylacetic acid (IBU) were obtained from Alfa Aesar (Germany). For regeneration and washing of the samples, the absolute isopropanol (iPrOH) (≥99,8%, 2-Propanol CP) from Biosolve BV(The Netherlands) were used. Carbon-dioxide (CO_2) cylinders (2.7, 50 L) with a purity of 99.5% from Linde Gas Benelux (The Netherlands) was used in the $scCO_2$ drying process. Gibco™ Dulbecco's modified Eagle's medium (DMEM) with 10% Gibco™ fetal calf serum (FCS) were purchased from Thermo Fisher Scientific (USA). For antibacterial studies, ampicillin and lysogeny broth (LB) medium which was created by a mixture of trypton (10 g /L), yeast extract (5 g/L), NaCl (5 g/L), and agar–agar (12 g/L) were all purchased from Carl Roth (Germany). *E. coli* was obtained from New England Biolabs (Germany) and *S. aureus* from DSMZ (German Collection of Microorganisms and Cell Cultures GmbH, Germany). Finally, all materials were used without further purification.

Fabrication of the aerogel fibers, textiles, and cylinders

Spinning dope

MCC and CHP were dried at 100 °C in a vacuum oven overnight to remove the moisture and achieve a constant weight. Two various spinning dopes of 10:1 and 5:1 of MCC:CHP were prepared using 60% zinc chloride (36 g), 31.66% of deionized water (19 mL), and 8.33% of polymer powders of MCC and CHP (5 g). Pure CLFs were fabricated by using 8.33% (5 g) of MCC. Homogenous clear solutions were achieved by dissolving the polymers at 75 °C and

using a mechanical stirrer (100 rpm) after approximately 90 min.

Wet spinning and washing

The spinning was done by a customized wet-spinning "DIENES LabLineCompact" unit as thoroughly explained previously (Rostamitabar et al. 2021c). In brief, monofilament alcogel fibers (fibers regenerated in alcohol) were obtained by spinning the dope through a spinneret with a capillary diameter of 330 µm in the iPrOH bath (30 L) without passing through an air gap between the nozzle and the regeneration bath. The pump rate of 1 mL/min and pressure of 2–3 bar were used. The fibers were collected in the coagulation bath on a porous stainless steel bobbin with a winding rate of 50 rpm. Fibers were washed in a customized soxhlet extractor system (NS 100) and the presence of salt leftovers was checked by conductivity meter and spot test as explained elsewhere (Rostamitabar et al. 2021b).

$scCO_2$ drying

The drying procedure was performed using $scCO_2$ dryer HPE 300 (EUROTECHNICA GmbH, Germany) at 130 bar and 50 °C over 45 min as described more completely elsewhere (Rostamitabar et al. 2021c).

Braided textiles

The dried fibers were manually turned into a braided construct containing at least 27 monofilaments in each mesh.

Aerogel cylinders

Cellulose and cellulose–chitosan cylinders were prepared in two different ratios of 10:1 and 5:1 (MCC:CHP) for density assessment and antibacterial assay. To obtain such cylinders, the warm solution was poured into cylindrical molds with an inner diameter of 14.5 mm and was centrifuged to remove air bubbles. Subsequently, they were regenerated in iPrOH and placed on a shaker (50 rpm) to increase the rate of solvent diffusion into the gel body. After 3 days and 6 cycles of solvent exchange, they were supercritically dried over 8 h in a similar condition to the fibers.

Post-treatment $scCO_2$ drug impregnation and drug loading efficiency

Post-treatment $scCO_2$ drug impregnation

30 ± 5 mg of IBU was placed at the bottom of the high-pressure vessel (V = 100 mL) with a magnetic bar. Then, 100 ± 10 mg of the dried aerogel fibers wrapped in filter papers were placed inside a porous cylinder that had a gap with the bottom of the vessel to avoid any contact between the fibers and the drug powders containing a rotating magnetic bar. A magnetic stirrer was placed under the vessel, and the pressure and temperature of CO_2 were set at 200 bar and 50 °C. After 24 h, the vessel was depressurized for over 60 min. Table 1 summarizes the fabricated samples and their corresponding abbreviation.

Drug loading efficiency

The drug loading efficiency (entrapment) of the post-treatment method (in $scCO_2$) was obtained by measuring the weight of the aerogel fibers before (M_i) and after (M_f) the impregnation as expressed by:

$$\textit{Drug loading efficiency}(\%) = \frac{M_i(g)}{M_f(g)} \times 100$$

Material and structural characterizations

Density and porosity

The porosity (Ø) was estimated from the bulk density and skeletal density as follows:

$$\text{Ø}(\%) = \frac{V_{\text{pores}}}{V_{\text{material}}} = 1 - \frac{\rho_{\text{bulk}}}{R \times \rho_{\text{skeletalCHP}} + (1-R) \times \rho_{\text{skeletalMCC}}} \times 100$$

where the skeletal density of cellulose ($\rho_{\text{skeletalMCC}}$) is 1.501 $g.cm^{-3}$ (Karadagli et al. 2015), the skeletal density of chitosan ($\rho_{\text{skeletalCHP}}$) is 1.42 $g.cm^{-1}$ (Bilbao-Sainz et al. 2017), and R is the ratio of CHP:MCC in the samples. The bulk density (ρ_{density}) was estimated as the mass to volume ratio of the three small cylindrical samples. The samples' diameters and lengths

were in the range of 0.75–1 cm and 2–2.2 cm, respectively. The dimension of the samples was measured by a digital vernier caliper.

Electron microscopy

The surface and cross-sectional morphologies of the aerogels were observed by using a Teneo scanning electron microscope (Thermo Fisher Scientific, USA). All fibers were broken in liquid nitrogen and coated with a 3 nm thick layer of iridium. Images were obtained using 5 kV voltage at a working distance of 10 mm. To obtain the average diameter of fibers SEM images were analyzed using Image J (version 1.8.0_172, NIH, USA). The diameter measurement was repeated 10 times at different points for each fiber.

Linear shrinkage ΔL of samples was determined from the SEM images by measuring the diameter of the samples after spinning (Di) and after drying (Df) using the following equation:

$$\Delta L(\%) = \frac{D_i - D_f}{D_i} \times 100$$

Elemental analysis

The nitrogen percentage in the CHCLAFs was quantified by elemental analysis using an Elemental Analyzer vario MICRO cube (Elementar, Germany). Sulfanilamide and helium were used as the calibration standard and carrier gas, respectively. The weight of the samples was 2–3 mg, and the total time of analysis was 10 min. The nitrogen content was converted to chitosan content (on a weight percentage basis, wt%) as described in the literature (Yen et al. 2009; Batista et al. 2020), and calculated as follows:

$$Chitosan(wt.\%) = \frac{P_N \times C}{N}$$

where P_N (wt.%) is the weight percentage of nitrogen in the fibers, C (g/mol) is the relative molecular weight of the chitosan repeating unit considering the deacetylation degree, and N (g/mol) is the molecular weight of elemental nitrogen.

FTIR

Fourier-transform infrared spectroscopy (FTIR) (Perkin Elmer, USA) was used to study inter/intra chemical interactions between the macromolecules. The spectrum was averaged over 32 spectra with a resolution of 2 cm^{-1} from a range of 4000 to 500 cm^{-1} in the reflectance mode.

X-ray diffraction

Wide-angle X-ray diffraction (WAXD) analysis on samples including microcrystalline cellulose powder and aerogel fibers was performed using a Ganesha diffractometer (SAXSLAB, Denmark) with a sample-to-detector distance of 116.536 mm. Cu Kα radiation (λ = 1.5406 Å) and silver behenate (d001 = 58.380 Å) were used for calibration, and samples were measured for 600 s. The diffraction spectrums were analyzed in transmission mode by saxsgui v2.23.23 software, and the environmental background was removed from the spectrums. The graphs were shown in the θ-2θ geometry.

TGA

The thermal properties of the aerogels were studied using a TA Q500 thermo-gravimetric instrument (TA Instruments, USA). Samples were heated from 20 °C to 500 °C with a rate of 10 °C min^{-1} under N_2 purge.

Nitrogen adsorption–desorption

Surface area and porosimetry measurements of the aerogel fibers were performed by ASAP™ 2020 (micrometrics, Norcross (Atlanta), GA, USA). Samples were degassed at 80 °C over 24 h and the Brunauer–Emmet–Teller (BET) method was utilized to determine the specific surface area. The pore volume and average pore size were obtained by Barrett-Joyner-Halenda (BJH).

Mechanical properties

The linear density, tensile strength, and elongation measurements of the fibers were analyzed using

Textechno Favimat + single fiber testing machine (Herbert Stein GmbH & Co., KG, Germany). The device was equipped with a load cell of 210 cN, and the linear density and tensile measurements were carried out at the rate of 10 mm/min. To address the coarse structure of the fibers and the resulting stiffness, high gauge lengths (20 mm) and high pretensions (0.1cN/dtex) using 20 samples per group were used.

In vitro characterization

Humidity absorbance and water uptake

Three replicates of braided fibers were dried in a vacuum oven at 90 °C for around 24 h to reach a constant weight. Subsequently, they were placed for 24 h in a humidity chamber at 25 °C with relative humidity (RH) of 50% and 80%. The weight of the samples was instantly measured before (W_{dry}) and after (W_{humid}) keeping it in the humidity chamber. Humidity absorbance weight ratio ($W_{RH\%}$) was measured by:

$$W_{RHX\%} = \frac{W_{humid} - W_{dry}}{W_{dry}} \times 100$$

Similarly, the dried braided fiber samples were placed in PBS solution (pH 7.4, 37 °C) and their weights were measured after removing the excess amount of water by filter papers. The wet weight (W_{wet}) was measured after 1, 8 and 24 h, and the water uptake (WU(%)) was calculated as below:

$$WU(\%) = \frac{W_{wet} - W_{dry}}{W_{dry}} \times 100$$

To investigate the water droplet sorption time on single aerogel fibers, three droplets with an approximate volume of 3 µL were placed on each fiber. Photographs were captured by FLIR chameleon®3 monochrome camera (1.3 megapixels) at four different time points of 5 s, 3 min, 5 min, and 10 min.

Wound exudate uptake

In order to investigate the capability of the braided structures to absorb wound exudate, the skin mimicking layers were created as explained in previous studies (Chen et al. 2016; Darpentigny et al. 2020). In summary, the artificial skin consisted of a dermis mimicking layer and an underneath hypodermis mimicking layer to avoid excessive drying over time was used as a skin model. The hypodermis was created by mixing gelatin (2 wt. %) and agar (0.4 wt.%) in deionized water on a heating stirrer at 50 °C and 100 rpm to achieve a homogeneous solution. The hot solution was poured into a cylindrical mold with an inner diameter of 75 mm to reach the height of 15 mm and left for 30 min to solidify. Similarly, the dermis layer made of gelatin (24 wt. %) and agar (2 wt. %) was subsequently poured on top of the hypodermis layer to reach a thickness of 5 mm and left to solidify. The braided structures were placed on the surface of the top layer and covered with parafilm tape. The weight of samples was measured at 8 different time points up to 48 h. The uptake weight percentage was reported based on WU (%), and the experiment was performed in triplicates.

Drug release

In vitro IBU release studies were performed in phosphate-buffered media of pH 7.4 using the dialysis bag technique similar to previously reported studies for wound dressing materials (Kevadiya et al. 2014; Ganesan 2017). Dialysis bags were equilibrated with dissolution medium for 2 h prior to the experiments. 100 ± 10 mg of CLF_{IBU}, $CH1CL10_{IBU}$, and $CH1CL5_{IBU}$ were suspended in dialysis bags containing 5 ml of release medium. Dialysis bags were dipped into the separate beakers containing 100 mL of PBS solution at 37 °C and stirred at a rate of 50 rpm. 12 samples over 72 h at various time intervals were measured as follows: 2 mL from the PBS and sample solution was transferred into a vial and subsequently, 2 mL of fresh PBS was added to the solution to maintain a constant medium volume. The measurements were performed in triplicate. Using a UV–visible UV3600 spectrophotometer (Shimadzu, Japan), the maximum absorption peaks (264 nm) for IBU in PBS solution and samples at different time intervals were measured. The Beer-Lambert law was utilized to obtain the concentration of the drug, and cumulative drug release was calculated by:

$$Q(\%) = \frac{C_n V + V_i \sum_{i=0}^{n-i} C_i}{M_f} \times 100$$

Q (%) is the percentage of the cumulative released drug, and V (mL) is the total volume of the samples. C_n (mg/mL) and V_i (mL) are the concentration and the volume of the samples taken at n and i time points. M_f (mg) is the weight of the loaded drug in the fibers, and the number of times that the drug release media is replaced is shown as n.

Cytotoxicity

Human dermal fibroblasts were isolated from the adult skin biopsies as previously described by Kreimendahl et al. (2019). Cells were cultured at 37 °C and 5% CO_2 in DMEM with 10% FCS. Cells at passage 4 were used for the viability experiment using XTT assay. The CLF and CHCLAF samples were sterilized in 70% ethanol and washed in PBS prior to the tests.

XTT assay was performed according to the ISO 10993–12. In short, aerogel fiber samples and negative control were incubated in a culture medium for 72 h. The negative control was a piece of polyethylene tube, and the positive control was DMSO. Cells were seeded in 96-well plates (1×10^4 cells per well) and were allowed to adhere to the wells for 24 h. After 24 h, cell medium was exchanged with the samples medium, positive control, and negative control or blank. After 1 day of incubation, the XTT assay was performed according to the manufacturer's protocol. The absorbance was measured in a multimode microplate reader M200 (Tecan, Switzerland) at 450 nm with a reference wavelength of 630 nm after 4 h of adding the salts to the cells. The assessment was performed in five replicates.

Antibacterial activity

Disk diffusion method

In order to keep a constant contact area of samples with agar diffusion disks, cylindrical geometries of cellulose and cellulose–chitosan aerogels were utilized. Diffusion disks were used for determining the antibacterial properties of the CHP and cylindrical aerogel samples. *Escherichia coli* DH5α and *Staphylococcus aureus* were grown on the nutrient agar slant and kept at 4 °C. Liquid cultures of both bacteria were inoculated from previously established cultures on lysogeny broth (LB) agar plates using 200 mL sterile LB medium with two different pHs of 5.8 and 6.3. The pH of the media was adjusted using a 1 M HCL solution before autoclavation. Cultures were incubated at 180 rpm and 37 °C for 16 h in a shaking incubator, and the agar plates were seeded with 0.1 mL of saturated bacteria suspension. Subsequently, a triplicate of cylindrical samples was placed on the agar plates with two different pHs. Ampicillin (100 µg/mL) was used as the positive control and non-treated plates as a negative control. Results were reported as the radius of the bacterial inhibition zone from the contact area with aerogel cylinders.

Table 1 The label of fiber samples was produced by using a spinning nozzle diameter of 330 (µm) and iPrOH as regeneration and washing solvent

Sample name	Cellulose ratio	Chitosan ratio	Loaded drug
CLF	1	0	–
CH1CL10	10	1	–
CH1CL5	5	1	–
CLF_{IBU}	1	0	ibuprofen
$CH1CL10_{IBU}$	10	1	ibuprofen
$CH1CL5_{IBU}$	5	1	ibuprofen

Determination of optical density of bacterial liquid cultures

This method was adopted from elsewhere (Heller and Spence 2019) to assess the antibacterial activity of the CHP and aerogel fiber samples. One colony from *E. coli* and *S. aureus* was scratched from their agar plate using a sterile pipette tip, and the pipette tip was ejected in a culture tube containing 5 mL of sterile LB medium with two different pHs of 5.8 and 6.3. Then, 20 mg of all samples were incubated in contact with the bacterial suspensions under orbital shaking (180 rpm) for 16 h at 37 °C. Ampicillin and sample-free bacterial tubes were used as the positive and negative control. The optical density (OD600) of the samples was measured in 96 well plates at a wavelength of 600 nm using Synergy™ HTX multi-mode microplate reader (BioTek, USA).

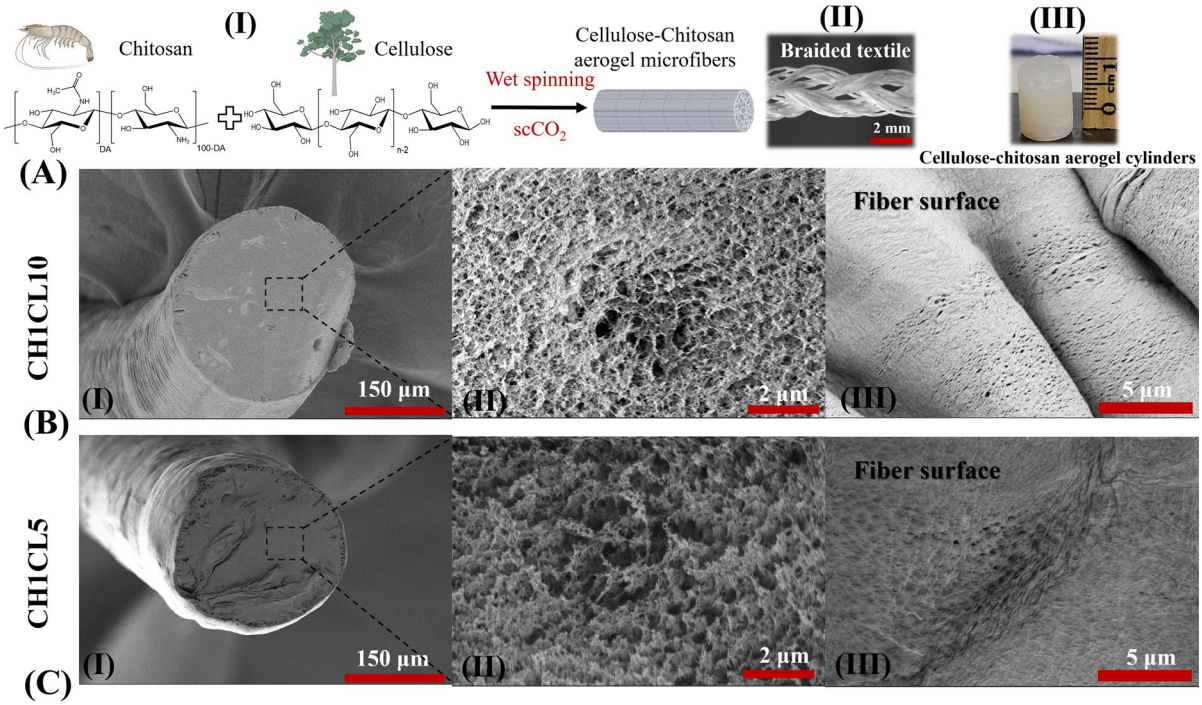

Fig. 1 **A** Fabrication process of chitosan-cellulose aerogel microfibers (I), a representative image of the chitosan-cellulose aerogel microfibers transformed into the braided textile (II) and examples of produced chitosan-cellulose cylindrical aerogel samples for density and porosity measurements (III). Cross-sectional morphology of the chitosan-cellulose fibers exhibiting a macro-porous outer shell (**B**-I, **C**-I) with a nano-porous inner core (**B**-II, **C**-II) of CH1CL10 and CH1CL5, respectively. Open porous surface of aerogel CH1CL10 fibers (**B**-III) and CH1CL5 fibers (**C**-III). Graphical elements were created using "BioRender.com"

Table 2 Linear diameter shrinkage (%) and textural properties of aerogel microfiber samples including estimated density (g/cm^3) and porosity (%) as well as BET surface area (m^2/g), BJH desorption pore volume (cm^3/g), and BJH desorption average pore diameter (nm)

Sample name	Linear shrinkage (%)	Density* (g/cm^3)	Porosity* (%)	Surface area (m^2/g)	Pore volume (cc/g)	Average pore width diameter (nm)
CLF	28.7 ± 1.1	0.18 ± 0.025	87.5 ± 1.7	127 ± 19	0.77 ± 0.15	9.28 ± 0.037
CH1CL10	20.4 ± 4.9	0.17 ± 0.012	88.4 ± 0.8	288 ± 10	1.14 ± 0.07	11.1 ± 1.053
CH1CL5	22.1 ± 2.1	0.19 ± 0.033	86.8 ± 2.2	305 ± 13	1.31 ± 0.04	11.06 ± .048

*Estimated for cylindrical geometries

Statistical analysis

All the experimental data are expressed as means ± standard errors (SD). The statistical analysis was done by Originlab software using a significance level of $p < 0.05$. Student t-test and one-way ANOVA based on the Tukey post hoc test were performed to determine the differences between different experimental groups.

Results and discussions

Fabrication and morphological characterization

After wet spinning, regeneration, washing, and scCO$_2$ drying processes, the aerogel fibers preserved their white and round cross-sectional shape. Fig. 1A-I shows the schematic of the fabrication process of

the CHCLAFs prepared from 8.3 wt. % of chitosan and cellulose. A representative example of manually braided textile produced from CHCLAFs consisting of a minimum of 27 monofilaments is shown in figure Fig. 1A-II. It also shows the flexibility and strength of the aerogel fibers which could be easily transformed into different textiles for practical applications. Fig. 1A-III is a representative photograph of light yellow cylindrical chitosan-cellulose aerogel fabricated for evaluation of density and antibacterial assessment. The density and porosity of cylindrical aerogel samples were estimated based on Eq. 2 and are shown in Table 2 No significant difference was observed between different samples.

The porous cross-section and surface morphologies of CH1CL10 and CH1CL5 aerogel fibers were revealed by SEM as shown in Fig. 1B-I, II and III and Fig. 1C-I, II and III, respectively. Cross-sectional pores consist of mesopores (2–50 nm) and macropores (> 50nm) according to the IUPAC classification. The fabricated aerogel fibers present good integrity and a wrinkled open porous surface. Both CHCLAF cross-sections consisted of a macroporous outer shell and a nano-porous inner core similar to the previously reported CLFs (Karadagli et al. 2015; Rostamitabar et al. 2021c). No significant difference between CHCLAF morphology is observable.

The CH1CL5 and CH1CL10 had a close linear shrinkage range of $20.4 \pm 4.9\%$ and $22.1 \pm 2.1\%$, respectively, based on the SEM images. This shrinkage could be attributed to the flexibility of the macromolecules chains of cellulose and chitosan that are slightly compacted during the regeneration process and also the removal of loosely packed fibrils of the gel matrix during washing of the fibers (López-Iglesias et al. 2019). The hybrid fibers showed lower shrinkage in comparison to the reported value for the pure CLF ($28.7 \pm 1.1\%$). This can arise from the chitosan interaction with the cellulose nano/microfibrils, which may affect the final physicochemical properties and network structure (Ul-Islam et al. 2011; Lin et al. 2013).

Structural and thermal properties

The elemental analysis proved the presence of nitrogen and chitosan in the structure of CHCLAFs. The CH1CL10 and CH1CL5 showed average nitrogen content of 0.59 ± 0.01 wt.% and 1.08 ± 0.01 wt.%, respectively. The calculated chitosan content was 7.23 ± 0.1 wt.% and 13.24 ± 0.1 wt.% for CH1CL10 and CH1CL5, respectively, indicating that both fibers had significantly different chitosan content.

Fig. 2A describes the FTIR spectra of polysaccharides and aerogel fibers. For all five samples, the broad bands at 3500–3100 cm^{-1} and 2800–2900 cm^{-1} were attributed to the –OH stretching and –CH stretching vibrations, respectively (Ul-Islam et al. 2011). In the case of chitosan powder and fibers, NH_2 groups have overlapped at the same range with –OH bands (Lin et al. 2012). Similarly, in all samples, C=O stretching and C–O stretching emerged at 1645–1650 cm^{-1} and 1014–1020 cm^{-1}. In the CHP, the characteristic amide groups of chitosan appeared at 1615 cm^{-1} (amide I), 1554 cm^{-1} (amide II), and 1380 cm^{-1} (amide III). Such peaks intensity decreased noticeably in the CHCLAFs. In the case of MCC and CHP in the range from 3000 to 3600 cm^{-1}, the band at 3300 cm^{-1} disappeared and the 3359 cm^{-1} band shifted to higher wavenumbers (3367 cm^{-1}). It has been reported that such phenomena can occur due to the intermolecular interaction between the OH and NH groups of cellulose and chitosan during the process of dissolution and regeneration (Lin et al. 2013; Yang et al. 2018). Overall, the FTIR spectra aided to confirm the presence of chitosan molecules in the CHCLAFs.

The XRD measurements were performed in order to investigate the microstructural changes in the CHCLAFs caused during processing. XRD patterns of MCC, CHP, CLF and blended aerogel microfibers are shown in Fig. 2B. MCC exhibited the peaks at $2\theta = 14.8°$, 16.4°, 20.4°, 22.7°, and 34.5° which were indexed as the cellulose crystalline plane (1–10), (110), (102)/(012), (200), and (004) (French 2014). The diffraction pattern of the CHP showed a prominent peak at 20.3° and was assigned to (1 1 0) as has been reported for chitosan (Kim et al. 2020). In the CLF, CH1CL10 and CH1CL5, remarkable changes were observed in their diffraction pattern of aerogels samples as the aforementioned peaks were transformed into a broad low-intensity peak between 15 and 20°. The results demonstrate that the crystal structure of the MCC and CHP was disrupted during the processes of dissolving in $ZnCl_2$ and regeneration in iPrOH. This is in accordance with some previous

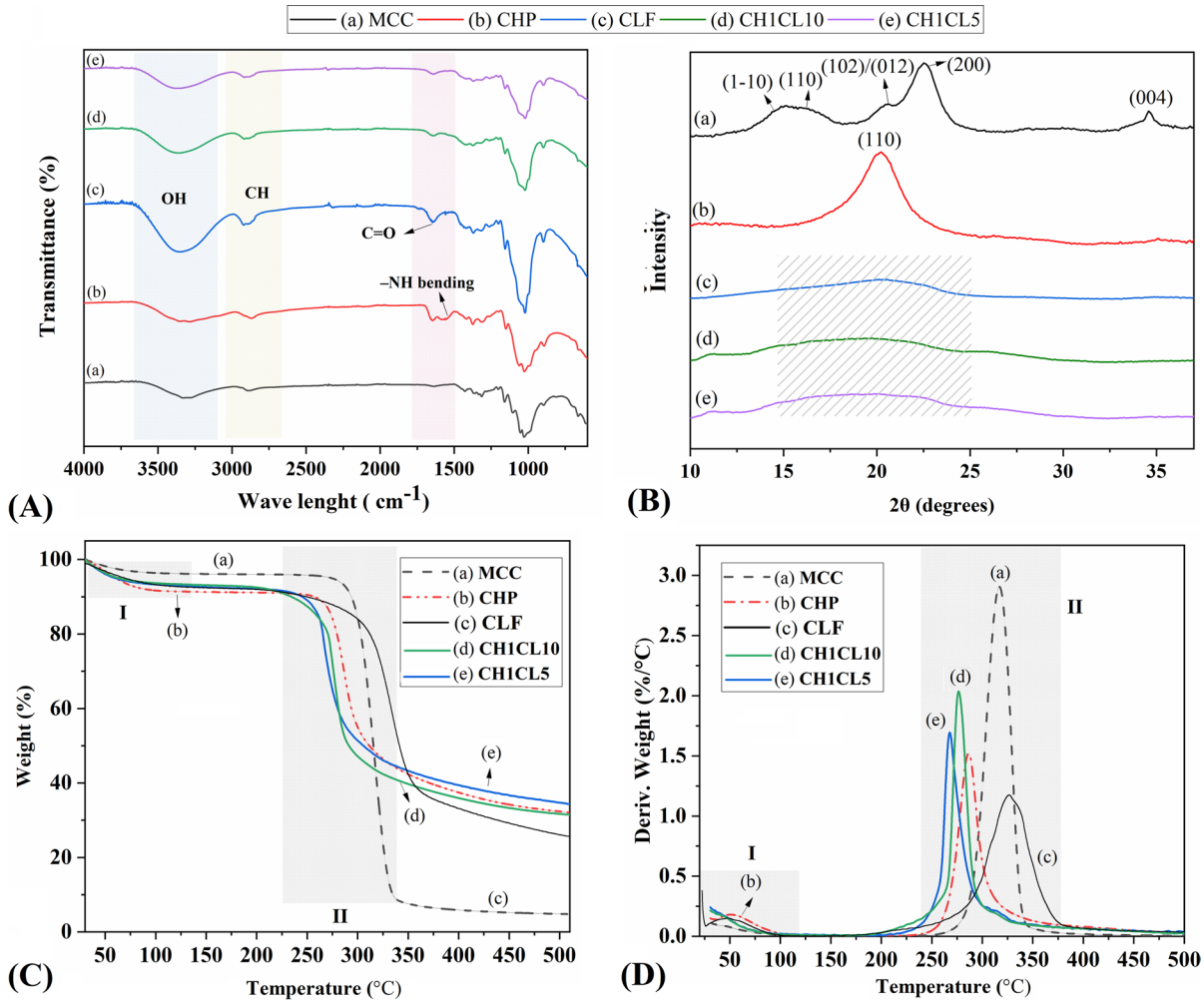

Fig. 2 **A** FTIR spectra of the MCC, CHP and aerogel microfiber samples indicating the presence of amide groups (–NH) in the blended aerogel fiber samples as well as the disruption of the crystalline structure of powders after dissolution and wet spinning. **B** XRD pattern of the MCC, CHP, and the aerogel fibers proving the amorphous structure (cross-hatched region) of the fabricated samples and the highly crystalline structure of the initial powders. **C** TGA graphs of the powders and aerogel fibers. The initial weight loss below 100 °C (I, cross-hatched region) arose from the vaporization of unbound and capillary water and the second step at 220–350 °C (II, cross-hatched region) was the relatively rapid decomposition of the cellulose and chitosan chains. Addition of chitosan to cellulose fibers decreased the thermal stability of fibers. **D** DTG of the powders and fibers showed that the decomposition range was broader and the rate was slower in the fibers; the chitosan addition increased the degradation rate in comparison to pure cellulose fibers

studies which showed that the dissolution in salt melt hydrate and blending MCC and CHP usually resulted in decreased crystallinity (Ul-Islam et al. 2011; Yang et al. 2018). The broad peaks of blended samples could be also attributed to the reformation of hydrogen bonds between cellulose and chitosan and support the FTIR results (Lin et al. 2012).

TGA graphs of initial materials and fabricated aerogel fibers are shown in Fig. 2C. The graphs exhibited the weight decline in two main steps. The initial weight loss below 100 °C arose from the vaporization of unbound and capillary water and the second step at 220–350 °C was the relatively rapid decomposition of the cellulose and chitosan chains. The results indicated that the thermal stabilities and onset thermal degradation of the MCC and CLF were inferior to those of the CHP and CHCLAFs.

The derivative thermogravimetry (DTG) curves are shown in Fig. 2D. In the first region (I), the increase of peak intensity and area demonstrated higher moisture uptake of the aerogel fiber samples apparently due to their porous nature providing a more accessible hydroxyl group for water molecules. The peaks in the second step (II) have shifted toward lower temperature and the peak area has decreased, which implies that the CHCLAFs exhibited a slower degradation rate compared to the MCC and CLF. These thermal stability data at high temperatures could be used to avoid degradation in aerogel samples involved in high temperature processes for instance heat sterilization or some characterization measurements such as high temperature degassing of samples before N_2 adsorption–desorption.

Therefore, it can be justified that the disrupted crystalline structure, addition of chitosan, and interactions between cellulose and chitosan chains after dissolving and processing in the $ZnCl_2$ solution affected the thermal decomposition properties of the fibers in comparison to macromolecular powders. Moreover, it was observed that the residual amount of the CHCLAF blend fibers escalated with the increase of the chitosan contents. This could be possibly explained by the greater interaction between amino groups of the chitosan and the hydroxyl groups of the cellulose as found in FTIR and XRD results (Lin et al. 2012).

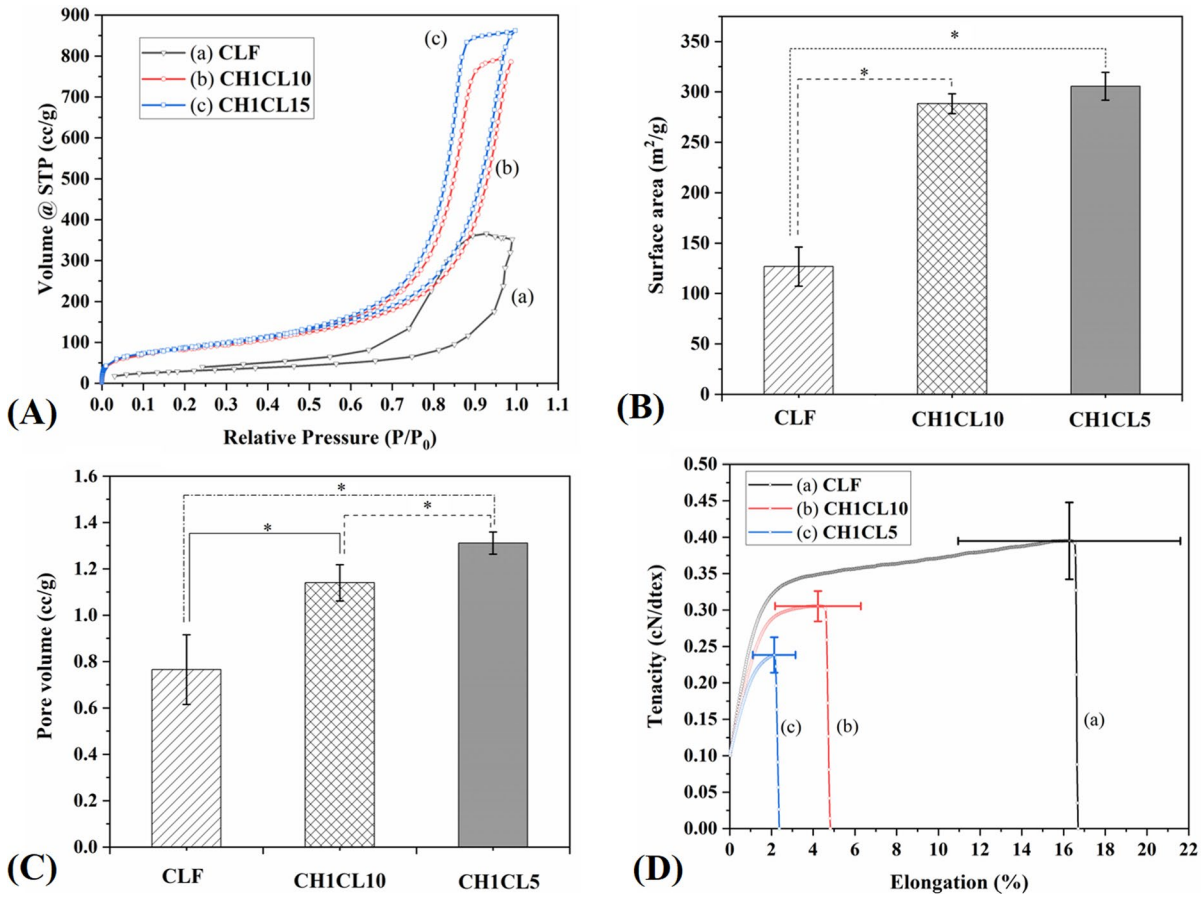

Fig. 3 **A** The N_2 adsorption–desorption isotherm curves of the aerogel fibers. **B** The BET specific surface area; the CHCLAFs showed a higher quantity than the CLFs. **C** BJH pore volume of aerogel fibers; fibers with higher chitosan quantity showed higher pore volume. **D** Representative curves of tenacity-elongation for the CLF, CH1CL10, and CH1CL5 with the maximum tenacity and the maximum elongation including the standard deviations. Addition of chitosan decreased the mechanical properties of the fibers. In all diagrams ($*p < 0.05$)

Textural properties of aerogel fibers

The N_2 adsorption–desorption isotherms of the aerogel fibers are displayed in Fig. 3A. The higher quantities of N_2 were absorbed in CHCLAFs compared to the CLFs. Nevertheless, the isotherms graphs for samples are comparable to IUPAC type IV with a hysteresis loop in the range of 0.7–1.0, representing the presence of meso- and macro-porous structure, which is pursuant to the SEM results (Reichenauer 2011; Rostamitabar et al. 2021c).

The textural properties including BET specific surface area (Fig. 3B), BJH desorption pore volume (Fig. 3C), and BJH desorption average pore width diameter of the aerogel fibers were analyzed by nitrogen adsorption–desorption. In general, the analyzed CHCLAFs possess surface area in the range of 288–305 m^2/g and pore volume in the range of 1.14–1.31 cm^3/g, comparable with the corresponding values for polysaccharide-based aerogels reported in the literature (Maleki et al. 2016; Soorbaghi et al. 2019). On the other hand, the reported value for CLFs surface area (127 ± 19 m^2/g) and pore volume (288–305 m^2/g) was noticeably lower than CHCLAFs. The average pore width diameter of the aerogel fibers is in the range of 9–12 nm. These results imply "no convection" effect since aerogel fibers' pore sizes are typically smaller than the mean free path of gas molecules (69 nm), making them interesting thermal insulation material (Zhang et al. 2021). Finally, the values of textural properties of aerogel microfiber samples is presented in Table 2.

The relatively higher specific surface area and pore volume of CHCLAFs in comparison to CLF could possibly be attributed to different macromolecule phases of the blend in the gelation and during the regeneration procedure (Zhang et al. 2021). However, such conclusions need further assessment of the current system by other techniques such as SAXS. In addition, in the majority of bioaerogel studies, the structure establishment is presumed to happen during solution gelation and/or solvent-exchange steps, and the subsequent $scCO_2$ drying leads to slight alterations. However, this has not been proven thoroughly and experimentally in most biopolymer systems and some recent studies challenge the common perception (Takeshita et al. 2019). Overall, the formation of porous structures is more complicated for hybrid aerogels from biomacromolecules and requires further research and it is not within the focus of the current study.

Mechanical properties

The CLF, CH1CL10, and CH1CL5 fibers showed maximum forces of 159 ± 14 cN, 123 ± 15 cN, and 56 ± 9 cN, respectively. Fig. 3D shows the representative curves of tenacity versus elongation (%) with an indication of standard deviation for the maximum tenacity (cN/dtex) and maximum elongation (%) of all fibers. The CHCLAFs exhibited a similar tensile profile in comparison to the previously disclosed assessments on CLFs in which an elastic region was followed by a plastic deformation until failure happened (Karadagli et al. 2015; Rostamitabar et al. 2021c). CLF, CH1CL10, and CH1CL5 exhibited maximum tenacity of 0.43 ± 0.052, 0.28 ± 0.021, and 0.24 ± 0.024 cN/dtex, respectively. The maximum elongation was 16.2 ± 5.33, 4.2 ± 2.06, and $2.1 \pm 1.02\%$ for CLF, CH1CL10 and CH1CL5, respectively.

In the CLFs, it has been observed that by increasing the initial cellulose concentration, the ultimate tenacity was enhanced which could be attributed to the increased amount of cellulose in the skeleton structure (Schestakow et al. 2016; Rostamitabar et al. 2021c). Furthermore, cellulose is well-known for its outstanding intrinsic mechanical properties with a theoretical modulus of about 100–200 GPa (~63–125 GPa g/cm^3) and tensile strength of about 4.9–7.5 GPa (~3.0–4.7 GPa g/cm^3) in its crystalline form. It has been reported that the addition of chitosan can lower the tensile strength of the blend due to the lower bonding strength of chitosan (Wu et al. 2004). In the case of CH1CL10 and CH1CL5, the cellulose amount was decreased and replaced by chitosan which consequently lowered the mechanical properties. This indicates that the blending ratio of hybrid aerogel fibers should be optimized based on the required textural and antibacterial properties without lowering their mechanical properties significantly.

The results also indicated that the maximum tenacity and elongation values had large standard deviations. One possible explanation could be the presence of the pores and wrinkles on the surface of fibers, minor diameter changes along the fiber axis, slight residual stiffness during the measurement, and variations in the structure of fibers. To enhance

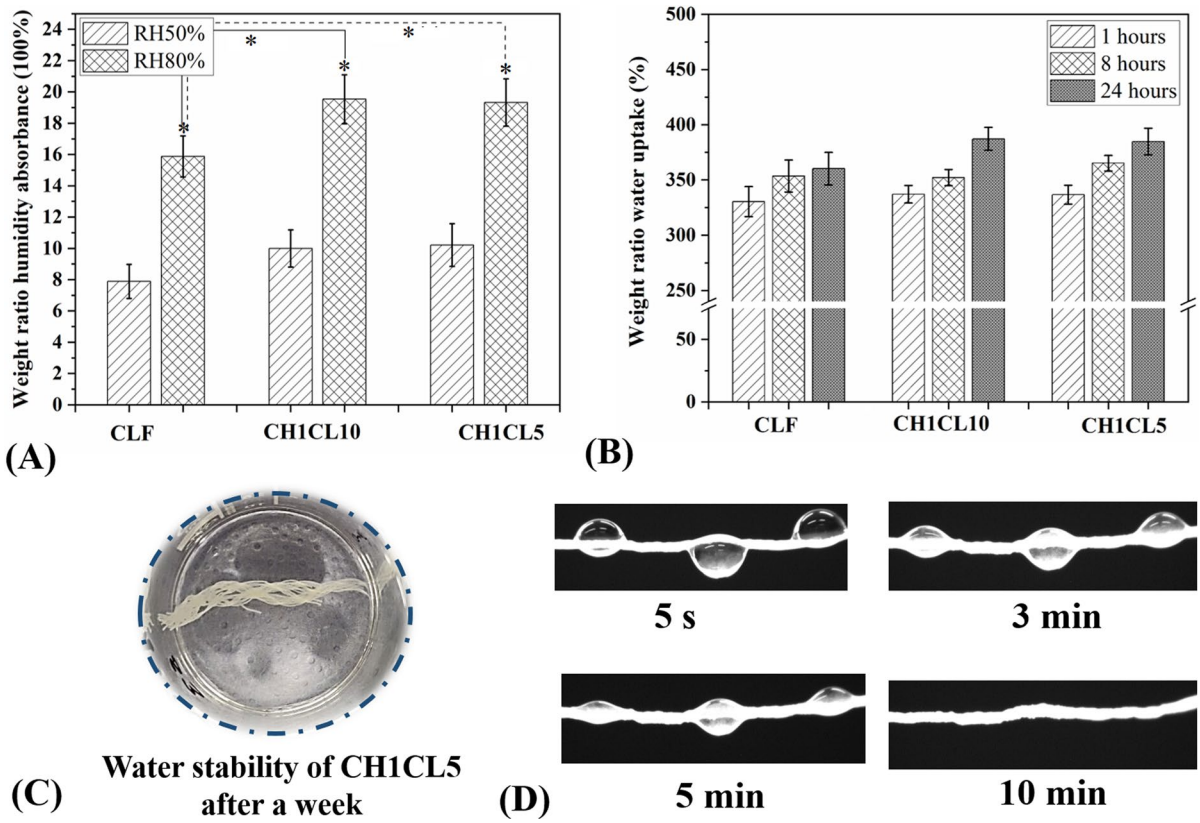

Fig. 4 **A** The humidity absorbance weight ratio of the aerogel fibers at 50 and 80 RH% after 24 h. **B** Water uptake of the braided aerogel fiber samples at 1, 8, and 24 h. **C** An exemplary image showing the wet stability of the CHCLAFs, CH1CL5 in this picture, after a week of being immersed in PBS. **D** Representative images of droplet sorption by aerogel fiber samples (here CH1CL5) at 5 s, 3, 5 and 10 min. In all diagrams (*$p < 0.05$)

the mechanical properties of the fibers, chemical crosslinking between hydroxyl groups of cellulose and chitosan could be performed utilizing solvent-free and non-invasive techniques to prevent the structural collapse of the fibers and prevent loss of amino groups, responsible for antibacterial activities.

Humidity, water and wound exudate uptake

The CHCLAF fibers exhibited a high moisture absorbance weight ratio due to the presence of accessible hydroxyl groups in their porous structure (Fig. 4A). Moreover, with increasing the relative humidity from 50 to 80% in all samples, the weight ratio of the adsorbed humidity increased; however, the absorbed amount of humidity by CLFs (15.8 ± 1.32 wt.%) was significantly lower than CH1CL10 (19.5 ± 1.57 wt.%) and CH1CL5 (19.3 ± 1.52 wt.%) at 80% RH. The lower pore volume of CLFs could be the main reason for the lower humidity absorption.

The water uptake capacity of the aerogel braided meshes was studied in PBS and results are shown in Fig. 4B. The PBS solution is utilized to simulate the human body fluid environment in terms of ion concentration and osmolarity. The water uptake for braided CHCLAF samples after 24 h of immersion (~400 wt.%) is slightly higher than the first hour. Although no striking difference is observed between various samples at similar time points.

Although crystalline domains of cellulose are inaccessible to water, non-crystalline domains are easily accessible to water. As shown in XRD results, the regenerated fibers were mainly in amorphous form, making them more susceptible to water absorption (Ioelovich 2011). Furthermore, despite differences

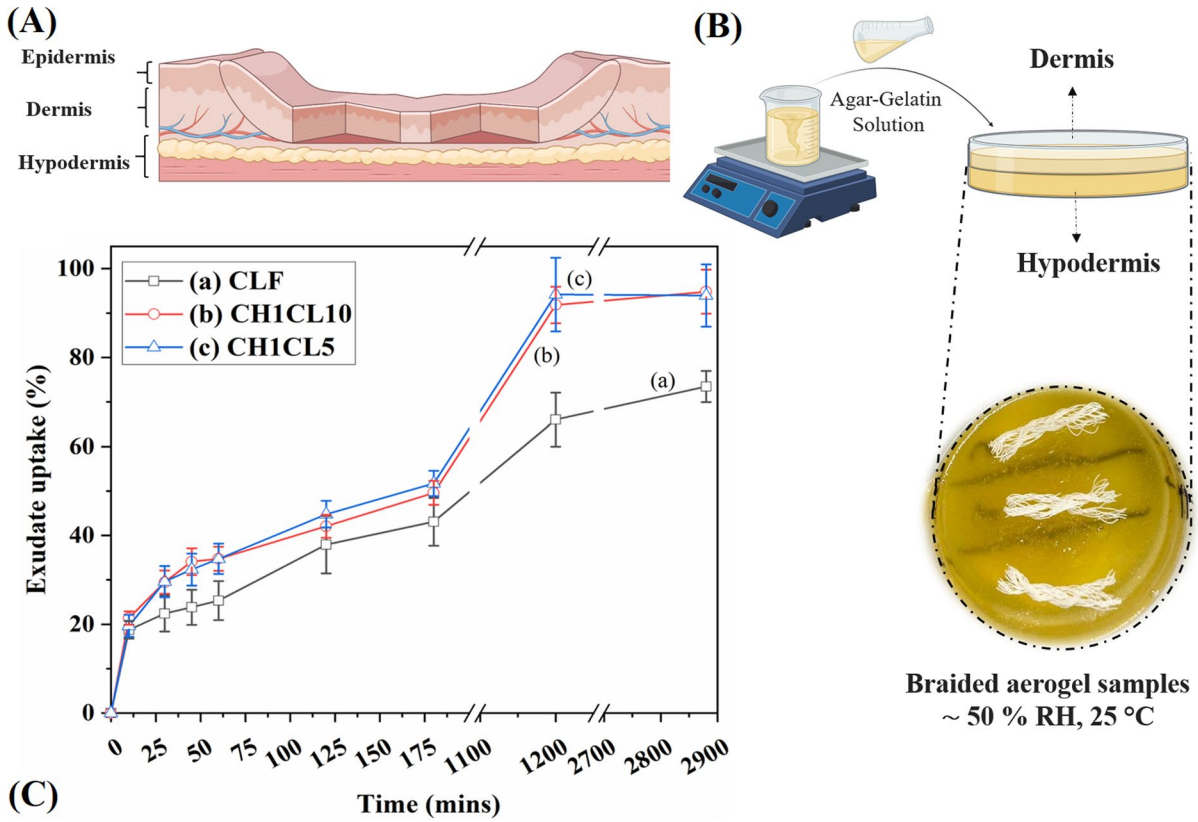

Fig. 5 **A** The graphical representation of the 3 skin layers. **B** Skin mimicking fabrication process and a photograph of the hypodermis and dermis layers in the dish including the braided meshes on the surface. **C** The exudate uptake graph for the aerogel braided samples exhibits better exudate uptake capability of the CHCL10 and CH1CL5 braided meshes compared to the CLF samples. Graphical elements were created with "BioRender.com"

in textural properties of aerogel fibers, their water uptake behavior was similar. This could be possibly because of the differences in the macrostructure of the braided patches rather than the microstructural properties of individual fibers as the water can be entrapped in between the filaments and thus have a huge impact on the final total weight.

Furthermore, fibers did not show any disintegration or matrix deterioration in PBS after 1 week (Fig. 4C). Droplet sorption by single aerogel fiber samples was observed by a macroscopic camera and all the samples absorbed the droplets completely after 10 min (Fig. 4D). These photographs also confirm that the measured time points in water uptake and humidity absorbance were long enough for fibers to get saturated with water molecules.

By using skin-mimicking layers, wound exudate uptake assessment on braided samples was conducted to simulate the in vivo conditions. A gel made of agar-gelatin with a hypodermis and a dermis mimicking layer was created as illustrated in Fig. 5A and B. In the first 3 h, a rapid exudate uptake up to 49.6 ± 2.71 and 51.7 ± 2.83 wt.% is observed for CHCL10 and CH1CL5 braided patches, respectively (Fig. 5C). Overall the uptake values were found to be lower for CLF mesh and it was 43.1 ± 5.36 wt.% after three hours. Following a rapid uptake of water in the structure, the rate declined and stabilized after 48 h. The maximum uptake of braided meshes was 73.4 ± 3.51, 94.8 ± 4.95, and 93.95 ± 7.01 for CLF, CHCL10 and CH1CL5 braided samples, respectively.

The exudate uptake values in comparison to water uptake ones were significantly lower due to

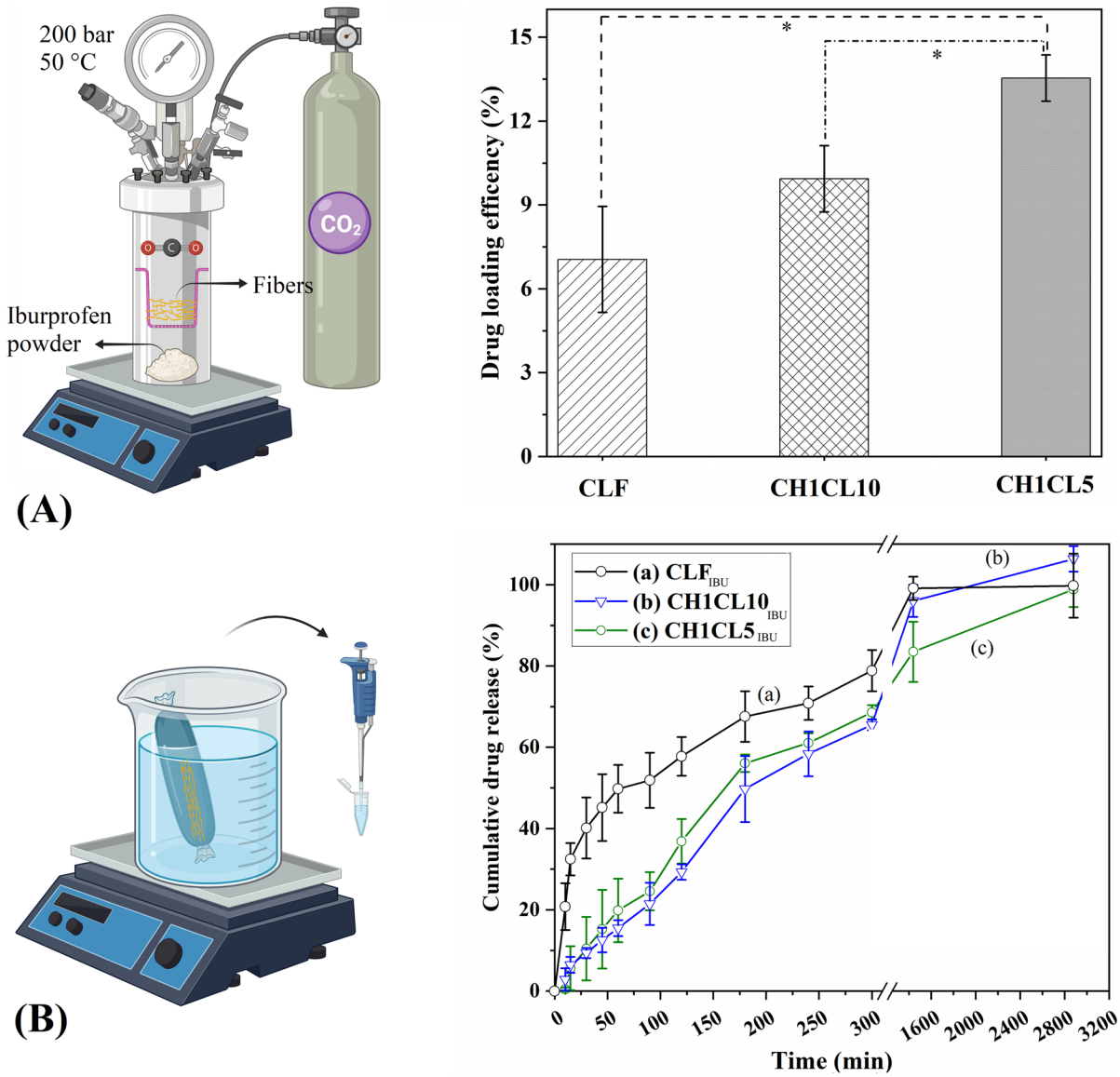

Fig. 6 **A** Post-treatment $scCO_2$ IBU loading of the aerogel fibers. The chitosan-cellulose fibers showed higher loading efficiency than pure cellulose aerogel fibers. **B** IBU release from CLF, CH1CL10, and CH1CL5. An improved sustained release profile was observed in CH1CL10 and CH1CL5 samples in comparison to the CLF samples. ($*p < 0.05$). Graphical elements were created using "BioRender.com"

the lower water accessibility and restricted diffusion of water molecules which occurs only through the surface that was in contact with the gelatin-agar layers. The CLFs presumably due to it is lower specific surface area and pore volume absorbed lower quantities of water in the wound exudate uptake test. Overall, it can be concluded that the CHCLAFs are better candidates than CLFs as wound dressing products since they can provide a moister environment at the wound site and absorb large amounts of exudate.

Drug loading efficiency and drug release profiles

Figure 6A displays the drug loading efficiency of aerogel fibers impregnated by the post-treatment technique. The highest entrapment values up to $13.54 \pm 0.825\%$ were achieved for CH1CL5. It is clear that IBU loading efficiency improved with the increase of aerogel fibers' surface area and pore volume. Such higher loading yield occurs based on a direct correlation between the impregnation efficiency and specific surface area, which is due to the amount of internal pores' surface available for drug deposition (Gurikov and Smirnova 2018; Groult et al. 2021).

The drug release profiles for CLF_{IBU}, $CH1CL10_{IBU}$, and $CH1CL5_{IBU}$ are shown in Fig. 6B $CH1CL10_{IBU}$ and $CH1CL5_{IBU}$ exhibited a similar and more sustained release profile in comparison to the $CLF_{IBU.}$ In the first hour, only 15.5 ± 1.97 and $21.4 \pm 5.18\%$ of IBU from $CH1CL10_{IBU}$ and $CH1CL5_{IBU}$, respectively, were released while CLF_{IBU} exhibited burst effect since $49.8 \pm 5.89\%$ was released. The drug eluted fractions for $CH1CL10_{IBU}$ and $CH1CL5_{IBU}$ were in the same range over the 600 min; however, after 24 h, the $CH1CL10_{IBU}$ drug release was slightly higher possibly due to a lower pore volume in comparison to $CH1CL5_{IBU}$. Also, CLF_{IBU} possessed significantly lower surface area and pore volume in comparison to $CH1CL10_{IBU}$ and $CH1CL5_{IBU}$ which could be the main reason for the observed burst effect.

As previously reported in the literature, loading of the IBU using post-treatment $scCO_2$ is mainly adsorbed on a molecular level. In comparison to other loading techniques, using the $scCO_2$ impregnation technique can be considered favorable to obtain targeted application products and sustained release (Smirnova et al. 2005; Mehling et al. 2009; García-González et al. 2011). In the case of CLFs and CHCLAF aerogels loaded by post-treatment $scCO_2$, no chemical interactions between the macromolecules and the drug can be noticed which have been confirmed by two main findings. First, the IBU release from the aerogels is complete, and the residual drug in the polymer matrix is negligible. Second, the IBU can be washed out from the aerogel networks by $scCO_2$ extraction (Groult et al. 2021).

The release rate from polysaccharide aerogels also depends on the stability of the aerogel matrix in the release medium. Since CHCLAFs exhibited very good dimensional stability in the wet environment even after a week, it makes them more suitable for drug delivery purposes compared to some polysaccharides reported from cellulose nanofibers (Darpentigny et al. 2020), and alginate and starch aerogel (Mehling et al. 2009). Moreover, the final aerogel wound dressing can be composed of CLFs and CHCLAF fibers with two different drug release profiles. For instance, fast local administration of the antibiotic at the wound site to prevent infections shortly after wound debridement can be obtained by antibiotic eluting from CLFs while longer sustained anti-inflammatory substances can be released via CHCLAF.

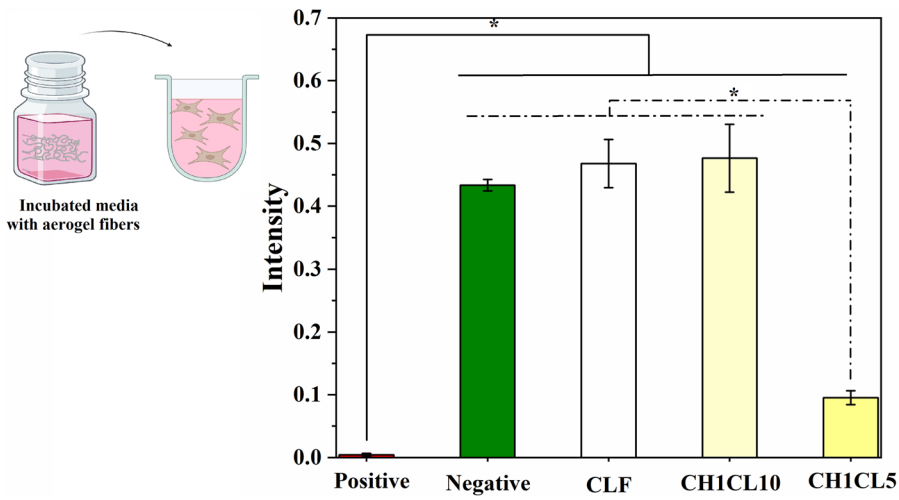

Fig. 7 XTT assay of the aerogel fibers; cell viability was observed in the samples on day 1 of the experiment. The negative sample was a piece of polyethylene and the positive sample was DMSO. (* data statistically significantly different, $p < 0.05$). Graphical elements were created with "BioRender.com"

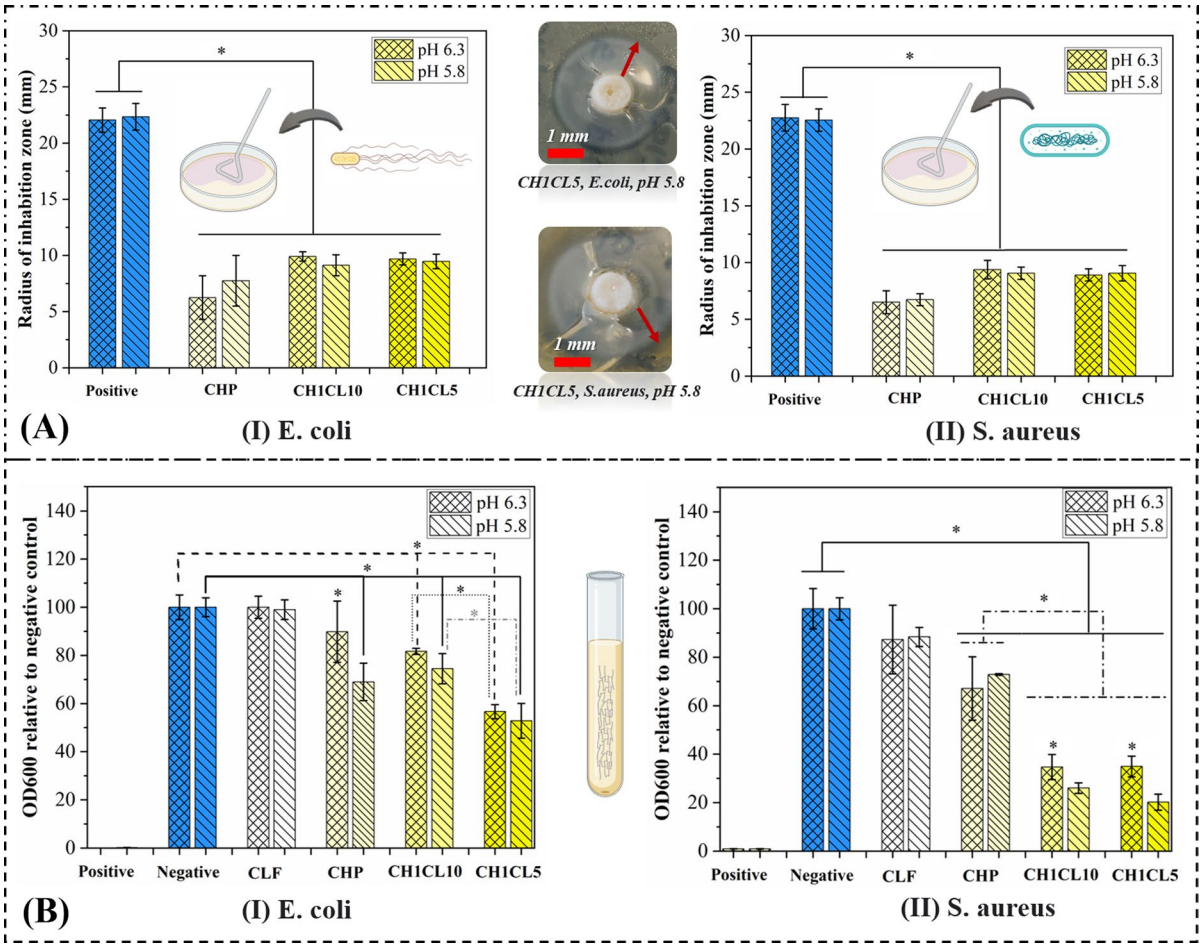

Fig. 8 **A** Disk diffusion antibacterial assessment of the CHP, CH1CL10 and CH1CL5 cylindrical aerogels against *E. coli* (I) and *S. aureus* (II). Chitosan containing cylindrical aerogel samples showed inhibition zone, and their performance was not different at two pHs of 5.8 and 6.3; however, cellulose cylinders did not show any antibacterial activity. **B** Liquid culture and the optical density (600 nm) of the CLF, CHP, CH1CL10, and CH1CL5 samples in the bacterial suspension of *E. coli* (I) and *S. aureus* (II). In both measurements, ampicillin was used as a positive control. Aerogel fibers containing chitosan showed inhibition activity while CLF did not show any antibacterial properties. In all diagrams (* data statistically significantly different, $p < 0.05$). Graphical elements were created with "BioRender.com"

Cytotoxicity

The human fibroblast cell viability was observed in the CLF, CH1CL5, and CH1CL10 samples after 1 day of cell culture demonstrating that the fibrous meshes provided suitable conditions for cell growth (Fig. 7). The increase of chitosan content in the CH1CL5 decreased the cell viability compared to the negative control, CLF, and CH1CL10 but was still significantly higher than the positive control. Even though these hybrid aerogel fibers have been produced for the first time, previously reported studies already proved the non-toxic nature of other types of chitosan-cellulose hybrid materials too (Naseri-Nosar and Ziora 2018; Fan et al. 2020).

In future studies, the cells viability dependency on chitosan concentration can be investigated comprehensively. In addition, in vitro and in vivo assays to analyze the effect of aerogel fibers on healing progression and rate in acute and chronic conditions

could also be performed to obtain a broader perspective about their wound dressing application.

Antimicrobial characteristics

Based on a disc diffusion method, the antibacterial activity of the powders and aerogel cylinders were tested by *E. coli* (Fig. 8A-I) and S. aureus (Fig. 8B-II) in two different pHs of 5.8 and 6.3. An inhibition zone up to approximately 10 mm was observed around the CHP and two chitosan-cellulose cylinders while no inhibition zone was spotted for the pure cellulose cylinder and therefore not shown in the diagram. No significant difference in inhibition radius zones of the CHP and cellulose-chitosan cylinders between pH 5.8 and 6.3 for both bacteria were detected.

Aerogel fibers and CHP antibacterial properties were also investigated in the bacterial suspension of *E. coli* (Fig. 8C-I) and *S. aureus* (Fig. 8D-II) at two different acidic pHs of 5.8 and 6.3. The Bacterial growth monitored by OD_{600} revealed that the CLFs in both pHs did not affect the *E. Coli* and *S. aureus* growth and had similar performance to the negative control. However, the bacteria proliferation significantly decreased in CH1CL10, CH1CL5, and CHP (except in *E. coli* and pH 6.3), in comparison to negative control in both pHs and bacteria. Although the CHP prevented the *E. Coli* growth significantly at the lower pH, *S. aureus* growth in the CHP suspension medium was not pH dependent. Moreover, CH1CL5 had higher *E. Coli* inhibition activity than CH1CL10 apparently due to the higher content of chitosan in the aerogel fiber matrix, but their activity did not seem to be different in various pHs. In the case of *S. aureus*, the antibacterial growth of CHP was lower in comparison to other aerogel fiber samples. Also at lower pH of 5.8, the CHCLAFs showed better antibacterial performance in comparison to pH 6.3. However, both CH1CL10 and CH1CL5 had a similar range of *S. aureus* inhibition activity in both pHs.

Though the exact antibacterial mechanism of chitosan is still debatable, many studies have suggested that the negatively charged cell wall of a bacterium can be disrupted by the chitosan protonated amino groups due to the interaction between opposite charges (Yilmaz Atay 2019). It is known that the chitosan's antimicrobial activity is influenced by several factors including the type of microorganism, the source of chitosan, temperature, molecular weight, degree of deacetylation and pH (Hosseinnejad and Jafari 2016). It has been proposed that the glucosamine monomer of chitosan obtains a positive charge (NH^{3+}) at the pH lower than 6.3–6.5 and that the antibacterial activity of chitosan increases as the pH decrease which can justify the higher *S. aureus* inhibition of the CHCLAFs in the lower pH media (Chang et al. 2015). Regarding *E. Coli*, CLCHAF bacterial inhibition did not seem to be pH dependent possibly due to the porous nature of the fibers which allows the amino groups to get protonated easier. Similarly, it can be the probable explanation for better performance of CHCLAFs in *S. aureus* in comparison to CHP in both pHs.

Traditional wound dressings mainly suffer from the lack of stability and the risk of infection. For instance, gram-positive bacteria, such as *S.aureus*, are mainly found in the initial stage of wound infection and are responsible for over 90% of infectious wound ulcers; however, gram-negative bacteria, such as *E.coli*, can be found when the wound is already developed (Boateng et al. 2008; Moeini et al. 2020). Therefore, due to favorable antibacterial properties of CHCLAFs, they can be considered as promising materials for wound dressing applications especially with the pathological acidic environment (pH < 6.3–6.5) of the infected chronic wounds. Future works can be devoted to loading the fibers with various antibiotics to increase the bactericidal activity and obtain pH nondependent patches.

Conclusion

Chitosan-cellulose aerogel microfibers have been prepared successfully by wet spinning of salt melt hydrate of $ZnCl_2$ and consequent $scCO_2$ drying. The CHCLAFs showed a low density (~0.18 g/cm^3), high porosity (~85%), and large specific surface area (~300 m^2/g) with a macro-porous outer shell and a nano-porous inner core. Better-sustained release of ibuprofen was observed in the CHCLAFs in comparison to the CLFs. Also, the CHCLAFs were non-toxic

and bactericidal against *E. Coli* and *S. aureus*. In Conclusion, addition of chitosan to cellulose in order to form hybrid aerogel microfibers led to a new class of wound dressing materials with significantly improved textural characteristics, antibacterial properties, and more sustained drug release behavior.

Acknowledgments The authors gratefully acknowledge the support of Hay Becker and Achim Besen (Aachen-Maastricht Institute for Biobased Materials, the Netherlands) in equipment upgrading and optimization as well as Hana Cvelbar for his assistance in performing the wet-spinning experiments. We appreciate the support of Christian Schmitz (Aachen-Maastricht Institute for Biobased Materials, the Netherlands) for antibacterial assessment. The authors also thank Dr. Ulrich Moerschel from Textechno Herbert Stein GmbH & Co.KG (Moenchengladbach, Germany) for his support in mechanical analysis

Author contributions All authors contributed to the study conception and design. Material preparation, data collection and analysis were performed by Matin Rostamitabar and Ailin Ghahramani. The first draft of the manuscript was written by Matin Rostamitabar and Samaneh Ghazanfari commented on previous versions of the manuscript. All authors read and approved the final manuscript.

Funding This project, as a part of the FibreNet consortium, has received funding from the European Union's Horizon 2020—Research and Innovation Framework Programme under the H2020 Marie Skłodowska-Curie Actions grant agreement No. 764713.

Declarations

Conflict of interest The authors have no relevant financial or non-financial interests to disclose.

References

Bano I, Arshad M, Yasin T, Ghauri MA, Younus M (2017) Chitosan: a potential biopolymer for wound management. Int J Biol Macromol 102:380–383. https://doi.org/10.1016/J.IJBIOMAC.2017.04.047

Batista MP, Gonçalves VSS, Gaspar FB, Nogueira ID, Matias AA, Gurikov P (2020) Novel alginate-chitosan aerogel fibres for potential wound healing applications. Int J Biol Macromol 156:773–782. https://doi.org/10.1016/J.IJBIOMAC.2020.04.089

Bilbao-Sainz C, Chiou B, Williams T, Wood D, Du WX, Sedej I, Ban Z, Rodov V, Poverenov E, Vinokur Y, McHugh T (2017) Vitamin D-fortified chitosan films from mushroom waste. Carbohydr Polym 167:97–104. https://doi.org/10.1016/J.CARBPOL.2017.03.010

Boateng JS, Matthews KH, Stevens HNE, Eccleston GM (2008) Wound healing dressings and drug delivery systems: a review. J Pharm Sci 97:2892–2923. https://doi.org/10.1002/JPS.21210

Chang SH, Lin HTV, Wu GJ, Tsai GJ (2015) pH Effects on solubility, zeta potential, and correlation between antibacterial activity and molecular weight of chitosan. Carbohydr Polym 134:74–81. https://doi.org/10.1016/J.CARBPOL.2015.07.072

Chen AI, Balter ML, Chen MI, Gross D, Alam SK, Maguire TJ, Yarmush ML (2016) Multilayered tissue mimicking skin and vessel phantoms with tunable mechanical, optical, and acoustic properties. Med Phys 43:3117–3131. https://doi.org/10.1118/1.4951729

Darpentigny C, Nonglaton G, Bras J, Jean B (2020) Highly absorbent cellulose nanofibrils aerogels prepared by supercritical drying. Carbohydr Polym 229:115560. https://doi.org/10.1016/J.CARBPOL.2019.115560

Dassanayake RS, Acharya S, Abidi N (2018) Biopolymer-based materials from polysaccharides: properties, processing, characterization and sorption applications. In: Edebali S (ed) Advanced sorption process applications, 1st edn. Intechopen, London, pp 1–24

Fan X, Li Y, Li X, Wu Y, Tang K, Liu J, Zheng X, Wan G (2020) Injectable antibacterial cellulose nanofiber/chitosan aerogel with rapid shape recovery for noncompressible hemorrhage. Int J Biol Macromol 154:1185–1193. https://doi.org/10.1016/J.IJBIOMAC.2019.10.273

French AD (2014) Idealized powder diffraction patterns for cellulose polymorphs. Cellulose 21:885–896. https://doi.org/10.1007/s10570-013-0030-4

French AD (2017) Glucose, not cellobiose, is the repeating unit of cellulose and why that is important. Cellulose 24:4605–4609. https://doi.org/10.1007/S10570-017-1450-3/FIGURES/3

Ganesan P (2017) Natural and bio polymer curative films for wound dressing medical applications. Wound Med 18:33–40. https://doi.org/10.1016/J.WNDM.2017.07.002

García-González CA, Alnaief M, Smirnova I (2011) Polysaccharide-based aerogels–Promising biodegradable carriers for drug delivery systems. Carbohydr Polym 86:1425–1438. https://doi.org/10.1016/J.CARBPOL.2011.06.066

Groult S, Buwalda S, Budtova T (2021) Tuning bio-aerogel properties for controlling theophylline delivery Part 1: Pectin aerogels. Mater Sci Eng C 126:112148. https://doi.org/10.1016/J.MSEC.2021.112148

Gurikov P, Smirnova I (2018) Amorphization of drugs by adsorptive precipitation from supercritical solutions: a

review. J Supercrit Fluids 132:105–125. https://doi.org/10.1016/J.SUPFLU.2017.03.005

Heller AA, Spence DM (2019) A rapid method for post-antibiotic bacterial susceptibility testing. PLoS ONE 14:e0210534. https://doi.org/10.1371/JOURNAL.PONE.0210534

Hosseinnejad M, Jafari SM (2016) Evaluation of different factors affecting antimicrobial properties of chitosan. Int J Biol Macromol 85:467–475. https://doi.org/10.1016/J.IJBIOMAC.2016.01.022

Ioelovich M (2011) Study of sorption properties of cellulose and its derivatives. BioResources 6:178–195

Karadagli I, Schulz B, Schestakow M, Milow B, Gries T, Ratke L (2015) Production of porous cellulose aerogel fibers by an extrusion process. J Supercrit Fluids 106:105–114. https://doi.org/10.1016/J.SUPFLU.2015.06.011

Kevadiya BD, Rajkumar S, Bajaj HC, Hettiar SS, Gosai K, Brahmbhatt H, Bhatt AS, Barvaliya YK, Dave GS, Kothari RK (2014) Biodegradable gelatin–ciprofloxacin–montmorillonite composite hydrogels for controlled drug release and wound dressing application. Colloids Surf B 122:175–183. https://doi.org/10.1016/J.COLSURFB.2014.06.051

Kim SJ, Hong BM, Park WH (2020) The effects of chitin/chitosan nanowhiskers on the thermal, mechanical and dye adsorption properties of electrospun PVA nanofibrous membranes. Cellulose 27:5771–5783. https://doi.org/10.1007/s10570-020-03191-w

Kreimendahl F, Marquardt Y, Apel C, Bartneck M, Zwadlo-Klarwasser G, Hepp J, Jockenhoevel S, Baron JM (2019) Macrophages significantly enhance wound healing in a vascularized skin model. J Biomed Mater Res A 107:1340–1350. https://doi.org/10.1002/JBM.A.36648

Lin S, Chen L, Huang L, Cao S, Luo X, Liu K, Huang Z (2012) Preparation and characterization of chitosan/cellulose blend films using $ZnCl_2 \bullet 3H_2O$ as a solvent. BioResources 7:5488–5499

Lin WC, Lien CC, Yeh HJ, Yu CM, Hsu SH (2013) Bacterial cellulose and bacterial cellulose–chitosan membranes for wound dressing applications. Carbohydr Polym 94:603–611. https://doi.org/10.1016/J.CARBPOL.2013.01.076

López-Iglesias C, Barros J, Ardao I, Monteiro FJ, Alvarez-Lorenzo C, Gómez-Amoza JL, García-González CA (2019) Vancomycin-loaded chitosan aerogel particles for chronic wound applications. Carbohydr Polym 204:223–231. https://doi.org/10.1016/J.CARBPOL.2018.10.012

Maleki H, Durães L, García-González CA, el Gaudio P, Portugal A, Mahmoudi M (2016) Synthesis and biomedical applications of aerogels: Possibilities and challenges. Adv Colloid Interface Sci 236:1–27. https://doi.org/10.1016/J.CIS.2016.05.011

McQueen RH (2011) Handbook of medical textiles. Woodhead Publishing, Cambridge

Mehling T, Smirnova I, Guenther U, Neubert RHH (2009) Polysaccharide-based aerogels as drug carriers. J Non Cryst Solids 355:2472–2479. https://doi.org/10.1016/J.JNONCRYSOL.2009.08.038

Minagawa T, Okamura Y, Shigemasa Y, Minami S, Okamoto Y (2007) Effects of molecular weight and deacetylation degree of chitin/chitosan on wound healing. Carbohydr Polym 67:640–644. https://doi.org/10.1016/J.CARBPOL.2006.07.007

Moeini A, Pedram P, Makvandi P, Malinconico M, Gomez d'Ayala G (2020) Wound healing and antimicrobial effect of active secondary metabolites in chitosan-based wound dressings: a review. Carbohydr Polym 233:115839. https://doi.org/10.1016/J.CARBPOL.2020.115839

Naseri-Nosar M, Ziora ZM (2018) Wound dressings from naturally-occurring polymers: A review on homopolysaccharide-based composites. Carbohydr Polym 189:379–398. https://doi.org/10.1016/J.CARBPOL.2018.02.003

Reichenauer G (2011) Structural characterization of aerogels. In: Aegerter M (ed) Aerogels Handbook, 1st edn. Springer, New York, pp 449–498. https://doi.org/10.1007/978-1-4419-7589-8_21

Ribeiro N, Soares GC, Santos-Rosales V, Concheiro A, Alvarez-Lorenzo C, García-González CA, Oliveira AL (2020) A new era for sterilization based on supercritical CO_2 technology. J Biomed Mater Res Part B Appl Biomater 108:399–428. https://doi.org/10.1002/JBM.B.34398

Rostamitabar M, Abdelgawad AM, Jockenhoevel S, Ghazanfari S (2021a) Drug-eluting medical textiles: from fiber production and textile fabrication to drug loading and delivery. Macromol Biosci 21:2100021. https://doi.org/10.1002/MABI.202100021

Rostamitabar M, Seide G, Jockenhoevel S, Ghazanfari S (2021b) Effect of cellulose characteristics on the properties of the wet-spun aerogel fibers. Appl Sci 11:1525. https://doi.org/10.3390/APP11041525

Rostamitabar M, Subrahmanyam R, Gurikov P, Seide G, Jockenhoevel S, Ghazanfari S (2021c) Cellulose aerogel micro fibers for drug delivery applications. Mater Sci Eng C 127:112196. https://doi.org/10.1016/J.MSEC.2021.112196

Sahana TG, Rekha PD (2018) Biopolymers: Applications in wound healing and skin tissue engineering. Mol Biol Rep 45:2857–2867. https://doi.org/10.1007/S11033-018-4296-3/TABLES/2

Schestakow M, Karadagli I, Ratke L (2016) Cellulose aerogels prepared from an aqueous zinc chloride salt hydrate melt. Carbohydr Polym 137:642–649. https://doi.org/10.1016/J.CARBPOL.2015.10.097

Sen CK (2019) Human wounds and its burden: an updated compendium of estimates. Adv Wound Care 8:39–48. https://doi.org/10.1089/wound.2019.0946

Smirnova I, Suttiruengwong S, Arlt W (2005) Aerogels: tailor-made carriers for immediate and prolonged drug release. KONA Powder Part J 23:86–97. https://doi.org/10.14356/KONA.2005012

Soorbaghi FP, Isanejad M, Salatin S, Ghorbani M, Jafari S, Derakhshankhah H (2019) Bioaerogels: synthesis approaches, cellular uptake, and the biomedical applications. Biomed Pharmacother 111:964–975. https://doi.org/10.1016/J.BIOPHA.2019.01.014

Sulaeva I, Henniges U, Rosenau T, Potthast A (2015) Bacterial cellulose as a material for wound treatment: properties and modifications. A review. Biotechnol Adv 33:1547–1571. https://doi.org/10.1016/J.BIOTECHADV.2015.07.009

Takeshita S, Sadeghpour A, Malfait WJ, Konishi A, Otake K, Yoda S (2019) Formation of nanofibrous structure in

biopolymer aerogel during supercritical co_2 processing: the case of chitosan aerogel. Biomacromol 20:2051–2057. https://doi.org/10.1021/acs.biomac.9b00246

Ul-Islam M, Shah N, Ha JH, Park JK (2011) Effect of chitosan penetration on physico-chemical and mechanical properties of bacterial cellulose. Korean J Chem Eng 28:1736–1743. https://doi.org/10.1007/S11814-011-0042-4

Ulker Z, Erkey C (2014) An emerging platform for drug delivery: aerogel based systems. J Control Release 177:51–63. https://doi.org/10.1016/J.JCONREL.2013.12.033

Wu YB, Yu SH, Mi FL, Wu CH, Shyu SS, Peng CK, Chao AC (2004) Preparation and characterization on mechanical and antibacterial properties of chitsoan/cellulose blends. Carbohydr Polym 57:435–440. https://doi.org/10.1016/J.CARBPOL.2004.05.013

Yang J, Kwon GJ, Hwang K, Kim DY (2018) Cellulose–chitosan antibacterial composite films prepared from LiBr solution. Polymers 10:1058. https://doi.org/10.3390/POLYM10101058

Yen MT, Yang JH, Mau JL (2009) Physicochemical characterization of chitin and chitosan from crab shells. Carbohydr Polym 75:15–21. https://doi.org/10.1016/J.CARBPOL.2008.06.006

Yilmaz Atay H (2019) Antibacterial activity of chitosan-based systems. In: Jana S (ed) Functional chitosan: drug delivery and biomedical applications, 1st edn. Springer, Singapore, pp 457–489

Yuan Z, Cheng J, Lan G, Lu F (2021) A cellulose/Konjac glucomannan–based macroporous antibacterial wound dressing with synergistic and complementary effects for accelerated wound healing. Cellulose 28:5591–5609. https://doi.org/10.1007/s10570-021-03821-x

Zhang S, He J, Xiong S, Xiao Q, Xiao Y, Ding F, Ji H, Yang Z, Li Z (2021) Construction and nanostructure of chitosan/nanocellulose hybrid aerogels. Biomacromol 22:3216–3222. https://doi.org/10.1021/acs.biomac.1c00266